# Dependence of small-scale energetics on large scales in wall-bounded flows

**By M. F. Howland AND X. I. A. Yang**

## 1. Introduction

Predicting small-scale turbulence using large-scales remains a focus of turbulence modeling. The underlying physical connection between large- and small-scale structures in a turbulent boundary layer has been studied in many different contexts, including but not limited to sub-grid scale modeling for large-eddy simulation (LES) (Moin *et al.* 1991; Meneveau & Katz 2000; Silvis *et al.* 2017), reduced-order modeling (Berkooz *et al.* 1993; Schmid 2010; McKeon 2017; Towne *et al.* 2017), and modeling of inter-scale interactions (Marusic *et al.* 2010; Mathis *et al.* 2011, 2013; Sidebottom *et al.* 2014).

In this work, we consider the inter-scale interaction known as amplitude modulation. Amplitude modulation refers to a specific inter-scale interaction in wall-bounded flows, where the small scales become more or less vigorous as a function of the large-scales (Brown & Thomas 1977; Rao *et al.* 1971; Hutchins & Marusic 2007; Mathis *et al.* 2009*a*). In high-Reynolds-number internal and external wall turbulence, streamwise elongated "superstructures" have been observed (Hutchins & Marusic 2007; Hutchins *et al.* 2011; Smits *et al.* 2011). The visibility of these structures in the energy spectrum increases as a function of Reynolds number (Hutchins & Marusic 2007; Hutchins *et al.* 2012). Motivated by this trend, Mathis *et al.* (2009*a*), as well as other previous investigators, hypothesized a scale separation between the small scale of the near wall cycle (Jiménez & Pinelli 1999) and the large scale of the superstructures. The long coherent superstructures modulate the amplitude of the near-wall energetics (Mathis *et al.* 2009*a*; Baars *et al.* 2015, 2017).

The phenomenological description of amplitude modulation has led to its incorporation into reduced-order modeling efforts. Amplitude modulation has been described by Marusic *et al.* (2010), as well as in a succession of later studies, predominantly in the predictive inner-outer (PIO) model as follows

$$u_i' = \alpha u_{o,L}' + [1 + \beta u_{o,L}'] u_{i,S}^*, \tag{1.1}$$

where $u_i'$ is the predicted streamwise velocity fluctuation at a near-wall location. All velocities, here and henceforth, are nondimensionalized in inner units. The subscripts $i$ and $o$ denote the inner and outer wall-normal locations. The subscripts $L$ and $S$ denote the large and small scales, respectively, and the superscript $'$ is used to indicate fluctuating quantities. The small and large scales are separated through filtration, which is typically performed in Fourier space. The effects of superposition and amplitude modulation are parameterized in $\alpha$ and $\beta$, respectively. The small-scale amplitude modulated signal is $u_{i,S}^*$. The large-scale amplitude modulating signal is $u_{o,L}'$. Motivated by the empirically observed scale separation, the distinction between small and large scales is set at a fixed length scale normalized by inner units (Mathis *et al.* 2009*a*, 2011). However, the coefficients $\alpha$ and $\beta$ and the signal $u_{i,S}^*$ must be empirically calibrated.

In Eq. (1.1), the amplitude modulation is assumed to be linear and symmetric. Ganapathisubramani *et al.* (2012) and Agostini & Leschziner (2014) have shown that the

amplitude modulation between the large-scale streamwise velocity and the small-scale energetics deviates from linearity away from the wall. As a result, we must relax the modeling constraints of Marusic, Mathis, and co-authors and rewrite Eq. (1.1) as

$$u' = u'_L + u'_S = u'_L + [1 + f(u'_L)]u^*_S. \tag{1.2}$$

Here, $u'_L$ and $u'_S$ are the small-scale and large-scale components, respectively, at a fixed wall distance. The small scale $u'_S$ is modeled as $u'_S = [1+f(u'_L)]u^*_S$, where the statistically universal fluctuating signal $u^*_S$ is the small-scale fluctuation in the absence of the influence of large scales (Marusic *et al.* 2010; Mathis *et al.* 2011, 2013). The response function $f(u'_L)$ characterizes the small-scale responses to the large scales, and is a generic function of the large-scale fluctuation $u'_L$. The response function $f = 0$ if the large and small scales are statistically independent. All quantities in Eq. (1.2) are functions of the wall-normal distance.

Here, we attempt to model $\alpha$ and $\beta$ without requiring arbitrary scale separation at a fixed length scale. Furthermore, we broaden our analysis of amplitude modulation without assuming linearity and attempt to explain the deviation from this response form $[f(u'_L)$ in Eq. (1.2)] away from the wall. The rest of this paper is organized as follows: in Section 1.1 we discuss both the previously used and presently proposed methods for quantifying amplitude modulation. In Section 2, we employ the recently developed hierarchical random additive process (HRAP) formalism to obtain the modeling parameters in the PIO model shown in Eq. (1.1). We show that the HRAP model is compatible with a generalized PIO with arbitrary scale separation. In Section 3, we measure the response of the small-scale energetics to the large-scale modulation without assuming linearity. Conclusions are given in Section 4.

### 1.1. *Quantifying amplitude modulation*

If $u^*_S$ and the response function $f(u'_L)$ are known and the large-scale fluctuation is resolved, Eq. (1.2) can be used to model the unresolved near-wall velocity fluctuation in wall-modeled large-eddy simulations (WMLES) according to

$$u'_i = \alpha u'_o + [1 + f(u'_o)]u^*_{i,S}, \tag{1.3}$$

where $u'_i$ is the near-wall streamwise velocity fluctuation (the inner fluctuation). Here subscripts $i$ and $o$ are used to denote inner and outer quantities, respectively. The large-scale velocity fluctuation at the inner location is approximated using the velocity fluctuation at a wall-normal distance further away from the wall $u'_o$ (outer fluctuation). As a result, the subscript $L$ is dropped since scale separation filtration is not performed. This choice is justified in the following discussion. The inner small-scale velocity fluctuation in the absence of the influence of large-scales is $u^*_{i,S}$. Again, all quantities in Eq. (1.3) are functions of wall-normal distance. In WMLES, $u'_i$ would be the unresolved near-wall velocity fluctuation, and it would be most practical (in complex flows for instance) to take $u'_o$ to be the velocity fluctuation at the first off-wall grid point (Bose & Park 2017), i.e., if the large scales are commensurate with the resolved eddies in WMLES (Sidebottom *et al.* 2014). If this is not possible, then Eq. (1.3) may be used only in *a posteriori* sense as in Inoue *et al.* (2012).

To determine $f(u'_o)$ and $u^*_{i,S}$, we need a characterization of small-scale energetics. A few characterizations of the small-scale energetics have been used in the context of inter-scale interaction modeling. Ganapathisubramani *et al.* (2012) and Agostini & Leschziner (2014) used $u'^2_S$. Mathis *et al.* (2009*a*) and Baars *et al.* (2015) used the envelope of the small scales $\mathrm{env}(u'_S)$ (the mean of $\mathrm{env}(u'_S)$ is removed). Since $u'^2_S$ and $\mathrm{env}(u'_S)$ yield

similar results, in this work, we follow Mathis *et al.* (2009*b*) and use $\mathrm{env}(u'_S)$, which is obtained by conducting Hilbert transformation of the small-scale signal. The response function $f(u'_o)$ is such that the signal computed according to

$$u^*_{i,S} = \frac{u'_i - \alpha u'_o}{1 + f(u'_o)} \tag{1.4}$$

is not modulated by the large scales such that

$$\left\langle \mathrm{env}(u^*_{i,S}) u'_o \right\rangle = 0. \tag{1.5}$$

Equation (1.5) provides only one constraint for the response function $f$ and allows only one parameter to be determined. The PIO model in Eq. (1.1) assumes $f(u'_o) = \beta u'_o$, which contains only one parameter. The PIO model also uses $u'_{o,L}$ instead of $u'_o$ (Mathis *et al.* 2011). Therefore, $\beta$ can be determined using Eq. (1.5).

In addition to providing a constraint for the response function, $\left\langle \mathrm{env}(u'_{i,S}) u'_o \right\rangle$ can be used to measure the response function directly. If the velocity fluctuation at an arbitrary wall-normal location can indeed be modeled using Eq. (1.2), it follows from Eq. (1.2) that

$$\langle \mathrm{env}_L(u'_S) |\, u'_L \rangle \approx f(u'_L), \tag{1.6}$$

where the response function also depends on the wall-normal location. We have assumed that $\mathrm{env}(u'_S) \approx 1 + f(u'_L)$. Here, a one-point correlation is used, so $i$ and $o$ are dropped and scale separation into $L$ and $S$ must be performed. If the response function is $f(u'_L) = \beta u'_L$, the amplitude modulation coefficient $\beta$ is positively correlated with the single-point correlation

$$R = \frac{\langle \mathrm{env}_L(u'_S) u'_L \rangle}{\mathrm{STD}[\mathrm{env}_L(u'_S)]\mathrm{STD}(u'_L)}. \tag{1.7}$$

In the above expression, $R$ is not precisely equal to $\beta$ because Hilbert transformation is an approximation of the small-scale envelope and $u'_{o,L}$ is an approximation of $u'_{i,L}$. This quantity $R$ has been used to quantify amplitude modulation in a number of previous studies (Hutchins & Marusic 2007; Mathis *et al.* 2009*a*; Baars *et al.* 2015). Agostini & Leschziner (2014) noted the likely influence of sweeps and ejections on quantifying amplitude modulation. In light of this claim and in anticipation of the results presented in the later sections, we further define

$$R_{>0} = \frac{\langle \mathrm{env}_L(u'_S) u'_L |\, u'_L > 0 \rangle}{\mathrm{STD}[\mathrm{env}_L(u'_S) |\, u'_L > 0]\mathrm{STD}(u'_L |\, u'_L > 0)}, \tag{1.8}$$

and similarly $R_{<0}$. If the response function is $f = \beta_{>0} u'_L$ for $u'_L > 0$, $R_{>0}$ is a measure of $\beta_{>0}$. Similarly, $R_{<0}$ is a measure of $\beta_{<0}$ if $f = \beta_{<0} u'_L$ for $u'_L < 0$. Notably, the correlation coefficient $R$ is most informative if the response function is linear, and $R_{>0}$ is most informative if the response function is linear for $u'_L > 0$ (similarly for $R_{<0}$). If the response function loses linearity, physical interpretations relying on $R$ (or $\beta$) become less clear.

## 2. Amplitude modulation and the hierarchical random additive process

In order to predict the parameters of Eq. (1.1), we use the HRAP formalism (Yang *et al.* 2016*a*,*b*,*c*; Yang & Lozano-Durán 2017). According to the HRAP formalism, the near-wall velocity may be modeled as

$$u'_i = a_1 + a_2 + ... + a_{N_i}. \tag{2.1}$$

We group the addends to large scales

$$u'_{i,L} = a_1 + ... + a_{N_o} \tag{2.2}$$

and small scales

$$u'_{i,S} = a_{N_o+1} + ... + a_{N_i}, \tag{2.3}$$

where $u'_i = u'_{i,L} + u'_{i,S}$. According to HRAP, $u'_{i,L}$ is also the velocity fluctuation at a wall-normal height $y_o \sim \delta/2^{N_o}$. Therefore, the large-scale fluctuation at a near-wall location may be modeled using velocity fluctuation at a wall-normal location further away from the wall. The distinction between the small- and large-scale components is arbitrary, and we require only $1 < N_o < N_i$.

We model $u'_S$ given $u'_L$. The subscript $i$ is dropped here for brevity. First, because $u'_S$ is fluctuation, $\left\langle u'_S \middle| u'_L \right\rangle = 0$. Second, the variance of $u'_S | u'_L$ is

$$\left\langle u'^2_S \middle| u'_L \right\rangle = \left\langle \left(a_{N_o} + ... + a_{N_i}\right)^2 \middle| u'_L \right\rangle \sim \left\langle u'^2_\tau \middle| u'_L \right\rangle \cdot \log\left(\frac{y_o}{y_i}\right), \tag{2.4}$$

where $y_i \sim \delta/2^{N_i}$. We have assumed that, given the large scales, the small scales are non-interacting. As a result, the large scales appear only in the normalizing velocity $u_\tau$ (which is the only relevant velocity scale near the wall). $\left\langle u'^2_\tau \middle| u'_L \right\rangle$ may be estimated by invoking the law of the wall

$$\left\langle u'^2_\tau \middle| u'_L \right\rangle = \left[\frac{\kappa[U(y_o) + u'_L]}{\log(y_o/\delta_\nu)}\right]^2, \tag{2.5}$$

where $U(y_o)$ is the mean velocity at the wall-normal height $y_o$ and $\delta_\nu$ is an inner length scale defined as $\delta_\nu = \nu/\langle u_\tau \rangle \exp(-\kappa B)$ for smooth walls. $B$ is the additive constant in the law of the wall. Equation 2.5 is often used in a wall-modeled LES context, where the wall-shear stress is modeled as a function of the velocity away from the wall (Bose & Park 2017). Equations Eq. (2.4)-(2.5) give estimates of the variance of $u'_S$. A similar procedure may be followed for estimates of higher-order moments, but for now we can model $u'_S$ as follows

$$u'_S \big| u'_L = u_\tau \cdot G(\mu, \sigma^2) = \frac{\kappa[U(y_0) + u'_L]}{\log(y_o/\delta_\nu)} G(\mu, \sigma^2), \tag{2.6}$$

where $G(\mu, \sigma^2)$ is a random variable whose mean $\mu$ and variance $\sigma^2$ are known. Equation (2.6) suggests that the amplitude modulation manifests through the modulation of the local Reynolds number and the local friction velocity, which is consistent with the interpretation provided by, e.g., Zhang & Chernyshenko (2016) and Baars *et al.* (2017). We can rewrite Eq. (2.6) as

$$u'^+_S \big| u'^+_L = \left[1 + \frac{1}{U^+(y_o)} u'^+_L\right] G(\mu, \sigma^2), \tag{2.7}$$

which conforms to Eq. (1.1), and provides us with a prediction of the modulation coefficient $\beta$,

$$\beta_{HRAP} = 1/U^+(y_o). \tag{2.8}$$

Equation leads to $\beta \approx 0.05$ for $y_o^+ \approx 400$ (Mathis *et al.* 2011), which agrees reasonably well with the measurements by Mathis *et al.* (2011). The superposition coefficient $\alpha = 1$ by the HRAP. Equation 2.6 is a fully predictive model. The usefulness of Eq. (2.6)-(2.8), however, relies on the response function being linear ($f = \beta u'_L$). The form of Eq. (2.8)

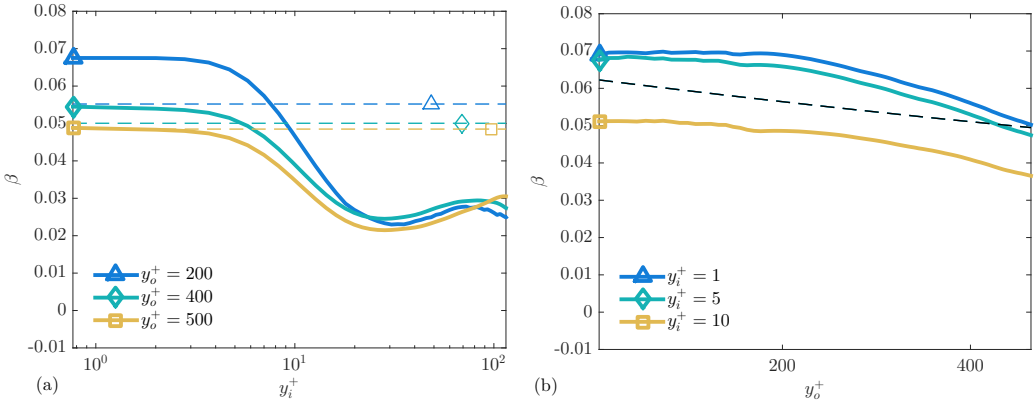


FIGURE 1. (a) The amplitude modulation coefficient $\beta$ as functions of $y_i^+$ for three outer locations, $y_o^+ = 200, 400$, and 500 ($y_o/\delta = 0.1, 0.2$, and 0.25). The $Re_\tau = 2000$ channel flow direct numerical simulation (Hoyas & Jiménez 2006) is used for the measurements. $\beta$, as suggested by Eq. (2.8), is indicated using dashed lines. (b) $\beta$ as functions of $y_o^+$ for $y_i^+ = 1, 5$, and 10.

suggests that amplitude modulation is invariant of the inner location and $Re_\tau$ (provided that $U^+(y_o^+)$ is fixed).

The response function is examined in detail in Section 3.1. For now, we only compare the prediction Eq. (2.8) with measurements taken from a $Re_\tau = 2000$ channel flow (Hoyas & Jiménez 2006) to study the usefulness of the assumed linear response function. Given an inner location and an outer location, and assuming the response function is $f = \beta u_o'$, the modulation coefficient $\beta$ can be computed using Eq. (1.4) and Eq. (1.5), where the large-scale velocity fluctuation at the inner location is approximated as $u_o = u_o'$. The velocities are low-pass filtered at the cutoff length scale $y$ at each wall-normal location to remove the small-scale, isotropic turbulence, whose significance is negligible at high Reynolds numbers. Figure 1 compares Eq. (2.8) with the measurements. Figure 1(a) shows $\beta$ as functions of the inner location for three outer locations, $y_o/\delta = 0.1, 0.2$, and 0.25. Figure 1(b) shows $\beta$ as functions of the outer location $y_o$ for three inner locations. We can make a few observations. Within the viscous sublayer, the modulation coefficient $\beta$ is approximately independent of the inner location, and the measurements agree reasonably well with Eq. (2.8). For $y_i$ within the viscous sublayer, Eq. (2.8) suggests that $\beta$ decreases as a function of $y_o$, and this is confirmed in Figure 1(b). However, the measurements do not follow Eq. (2.8) beyond the viscous sublayer. As $y_i^+$ is increased beyond $y_i^+ \approx 10$, $\beta$ is poorly predicted in magnitude and in scaling with respect to $y_o^+$.

The usefulness of Eq. (2.8) relies crucially on the response function being linear. The failure of Eq. (2.8) outside the viscous sublayer suggests either that the response function $f$ may only be linear in the viscous sublayer or that the modeling framework breaks down. In Section 3, we will quantify deviations from a linear response function in wall-bounded turbulence.

## 3. Small-scale responses to large-scale fluctuation

In this section, we directly measure the response function according to Eq. (1.6). We will also discuss the physical implications of the empirical form of the response function.

### 3.1. *Empirical response function*

We measure the response function using high-Reynolds-number boundary-layer measurements at friction Reynolds numbers $Re_\tau = 6500, 10000$, and 13000. Details of these data can be found in Hutchins *et al.* (2009) and Talluru *et al.* (2014). We focus on spatial amplitude modulation (Yang & Howland 2018); therefore, the local instantaneous velocity is used as the convective velocity. We follow Mathis *et al.* (2009*a*) and define the large and small scales on the basis of pre-specified length scale, $l^+ = 4000$.

Figure 2(a-c) shows $\langle \mathrm{env}_L(u'_S)|u'_L\rangle$ (i.e., the response function) as functions of the large-scale velocity fluctuation at three wall-normal locations, $y^+ \approx 5$, $y^+ \approx 75$, and $y^+ \approx 200$. The mean of $\langle \mathrm{env}_L(u'_S)|u'_L\rangle$ is removed for visualization. Results of channel flow at $Re_\tau = 2000$ and 5200 (Hoyas & Jiménez 2006; Lee & Moser 2015) are included for comparison. The direct numerical simulation (DNS) results agree reasonably well with the results obtained using the hot-wire data at similar Reynolds numbers (DNS, $Re_\tau = 5200$; hot-wire, $Re_\tau = 6200$). Thus, we may conclude that spatial amplitude modulation is correctly measured using the proposed conversion of Yang & Howland (2018). We make a few observations. First, the response functions at different Reynolds numbers collapse at the same $y^+$ in the near-wall region. A slight discrepancy is noted for the $Re_\tau = 2000$ channel results, which is likely due to finite Reynolds number effects. Second, the response function is approximately linear and symmetric within the viscous sublayer ($y^+ < 5$). Third, in the buffer and log layers, the small-scale fluctuation responds asymmetrically to the large-scale fluctuation depending on whether $u'_L$ is positive or negative. $\langle \mathrm{env}_L(u'_S)|\, u'_L\rangle$ and $u'_L$ are positively correlated for $u'_L < 0$ (positive amplitude modulation), but for $u'_L > 0$, they become negatively correlated (negative amplitude modulation). The response function $f(u'_L)$ is approximately positive and linear for $u'_L < 0$ and negative and linear $u'_L > 0$, respectively. The presence of negative amplitude modulation, i.e., less energetic small scales being correlated with positive large-scale fluctuation and vice versa, was discussed by Baars *et al.* (2017). These authors argued that such a behavior is the result of intrusions of none/less-turbulent flows from the bulk region into the near-wall region. As flows in the bulk tend to be at high speeds (i.e. $u'_L > 0$), Figure 2 is consistent with the argument proposed by Baars *et al.* (2017). Figure 3(a-c) shows $\langle \mathrm{env}_L(u'_S)|u'_L\rangle$ at wall-normal locations $y/\delta \approx 0.1$, 0.2, and 0.4. Again, the response functions collapse in the log region at the same $y/\delta$ locations for all $Re_\tau$ considered in the present study. The response function is nearly linear in the bulk region. In particular, the same slope manifests at the different wall-normal locations in the log layer. Characterized spatially, amplitude modulation is not a function of $Re_\tau$ for the Reynolds numbers considered in the present study in the near-wall or in the bulk regions provided that the small and large scales are adequately separated and inner units are used. These observations are qualitatively consistent when the small-scale energetics are measured using $u'^2_S$ (or $|u'_S|$).

The correlation coefficient $R$, as defined in Eq. (1.7), is most informative when the response of small scales to large scales is captured by a linear and symmetric response function for all $u'_L$. In such a case, $R \sim \beta$. A more detailed quantification of the amplitude modulation is provided in Figure 2(a-c) and Figure 3(a-c), which directly examine the response function. According to Figure 2, the response function $f(u'_L)$ is approximately linear for $< 0$ and $> 0$. As such, we may condition the response function as

$$f(u'_L) = \beta_{<0} u'_L, \quad \text{for} \quad u'_L < 0; \quad f(u'_L) = \beta_{>0} u'_L, \quad \text{for} \quad u'_L > 0. \tag{3.1}$$

According to Figure 2, $\beta_{<0} \approx \beta_{>0}$ in the viscous sublayer and in the bulk region. Both

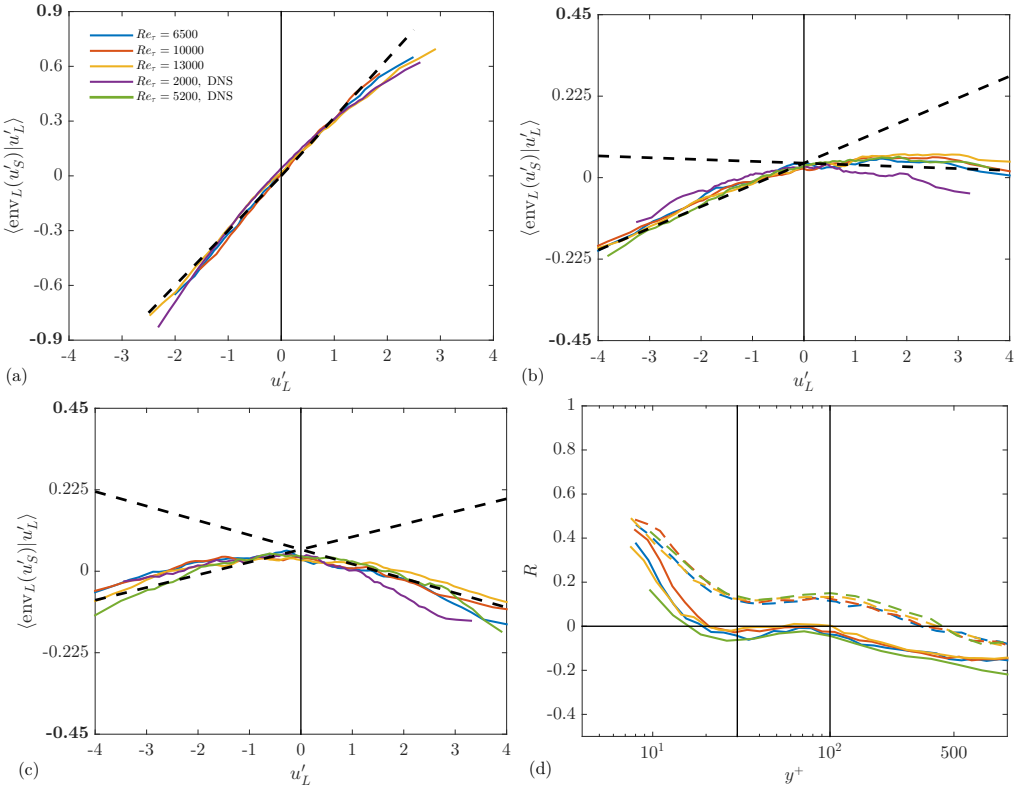


FIGURE 2. Conditionally averaged energy content at small scales $\langle \mathrm{env}_L(u'_S)|u'_L\rangle$ as functions of the large-scale fluctuation $u'_L$ at wall-normal locations (a) in the viscous sublayer ($y^+ \approx 5$), (b) in the buffer layer ($y^+ \approx 75$), (c) in the log layer ($y^+ \approx 200$). Dashed lines are linear fits of the data for $u'_L > 0$ and $u'_L < 0$, respectively. The slopes for $u'_L > 0$ are (a) 0.32, (b) -0.01, and (c) -0.04. The slopes for $u'_L < 0$ are (a) 0.32, (b) 0.06, and (c) 0.04. The solid vertical line indicates $u'_L = 0$. The $y$-scale is magnified in (b) and (c) for better visualization. (d) $R_{\lessgtr 0}$ as functions of $y^+$. Solid lines represent $R_{>0}$ are solid lines and dashed lines represent $R_{<0}$. Solid vertical lines represent the buffer layer of $30 < y^+ < 100$.

$\beta_{<0}$ and $\beta_{>0}$ decrease monotonically as functions of the wall-normal distance. If Eq. (3.1) is an accurate approximation of the response function, $R_{<0}$ and $R_{>0}$ as defined in Eq. (1.8) are direct measures of $\beta_{<0}$ and $\beta_{>0}$ as functions of the wall normal distance. Figure 2(d) shows $R_{<0}$ and $R_{>0}$ as functions of the wall-normal distance for boundary-layer and channel flows at various Reynolds numbers as functions of $y^+$, and Figure 3 shows the same quantities as a function of $y/\delta$. Within wall-normal distances where viscous effects dominate, $\beta_{<0} \approx \beta_{>0}$ and $R_{<0} \approx R_{>0}$. This also manifests in the bulk region, where viscosity is not dominant. In the viscous region, $R$ and $\beta$ are positive. In the bulk region, $R$ and $\beta$ are negative. $R_{>0}$ decreases to zero at $y^+ \approx 20$, and $R_{<0}$ is greater than 0 for wall-normal distances $y^+ \lesssim 500$. Notably, $R_{<0} \approx R_{>0} \approx Const.$ in the bulk region, as is expected from Figure 3 (a-c).

If the response function follows Eq. (3.1), we can compute $\beta_{<0}$ and $\beta_{>0}$ in a similar manner as $\beta$ in Eq. (1.1) was computed, except that here the constraint Eq. (1.5) is

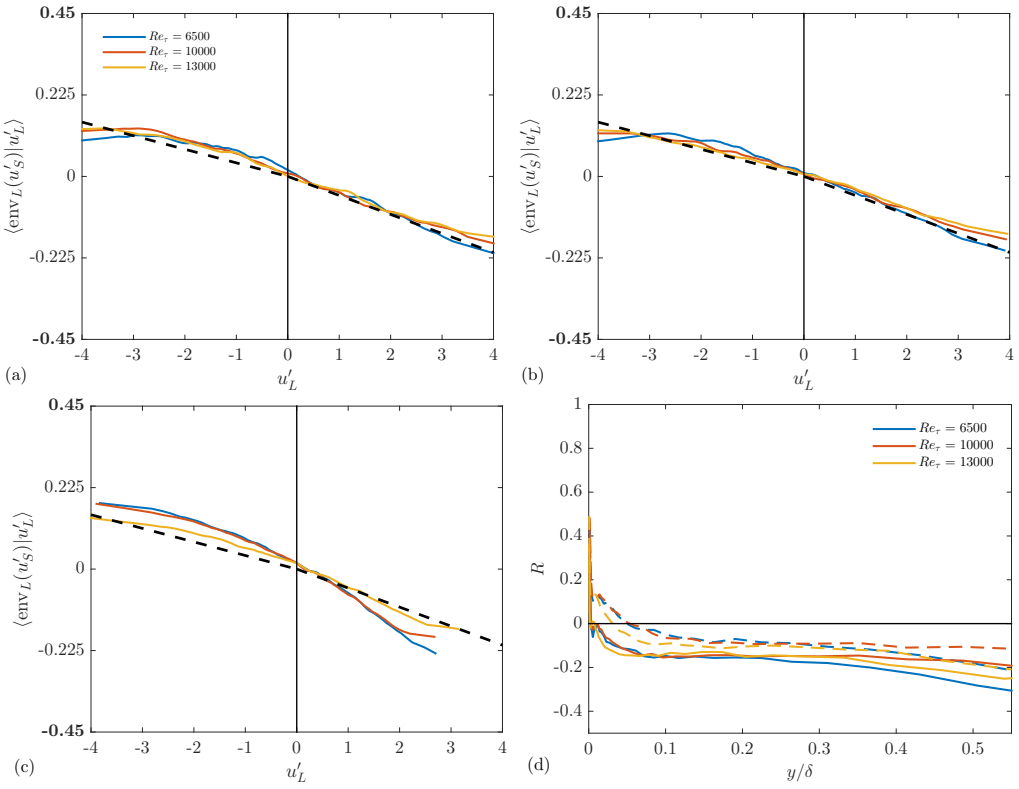


FIGURE 3. Conditionally averaged energy content at small scales $\langle \mathrm{env}_L(u'_S)|u'_L\rangle$ as functions of the large-scale fluctuation $u'_L$ at wall-normal locations in the bulk region ($y/\delta = 0.1$ (a), 0.2 (b), and 0.4 (c)). Dashed lines show linear fits for the present data. The slope for $u'_L > 0$ is $-0.05$ for (a-c). The slope for $u'_L < 0$ is $-0.04$ for (a-c). The linear fits are held constant for all $y/\delta$ shown. The solid black line indicates $u'_L = 0$. (d) $R_{\lessgtr 0}$ as functions of $y/\delta$. Solid lines represent $R_{>0}$, and dashed lines represent $R_{<0}$.

applied for $u'_L < 0$ and $u'_L > 0$, respectively

$$\left\langle \mathrm{env}_L(u^*_{i,S,m})u'_o \middle| u'_o \lessgtr \right\rangle = 0. \tag{3.2}$$

$f(u'_o)$, as defined in Eq. (3.1) is such that the universal signal computed according to

$$u^*_{i,S,m} = \frac{u'_i - \alpha u'_o}{1 + f(u'_o)}, \tag{3.3}$$

truly satisfies Eq. (3.2). The subscript m denotes a parameter that requires modeling. In Eq. (3.2)-(3.3), we have added the subscript $m$ to indicate that in the context where those parameters are desired, the large scales and the universal de-modulated signals will need to be modeled. Equation (3.2) provides two constraints and allows the two parameters $\beta_{<0}$ and $\beta_{>0}$ in Eq. (3.1) to be determined. The prediction of Eq. (2.8) can also be updated to account for the noted asymmetry in the response function

$$\beta_{\lessgtr 0} = 1/\left\langle U^+(y_o) + u'_o \middle| u'_o \lessgtr 0 \right\rangle. \tag{3.4}$$

A consequence of Eq. (3.4) is that the predicted amplitude modulation is stronger for neg-

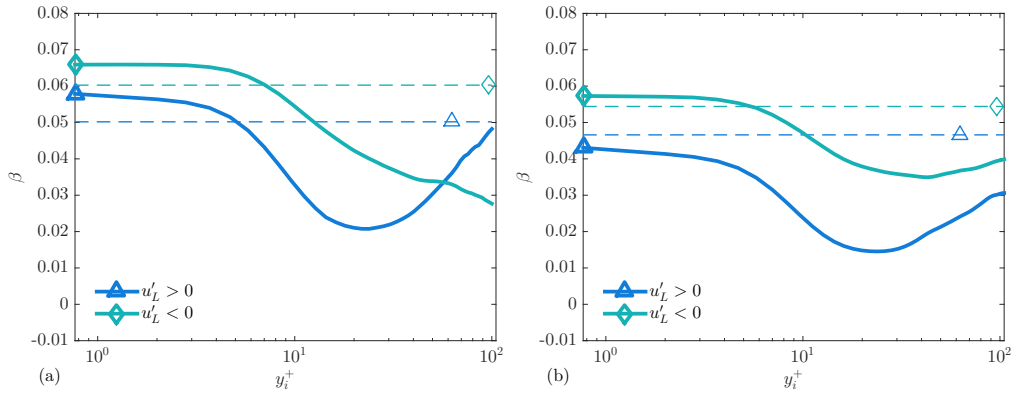


FIGURE 4. $\beta_{\lessgtr}$ [measured according to Eqs. (3.2)-(3.3)] as functions of $y_i^+$ for channel flow at $Re_\tau = 2000$ (solid lines). Dashed lines represent the predictions using Eq. (3.4). (a) for $y_o^+ = 215$ and (b) for 400.

ative large-scale fluctuation than for positive large-scale fluctuation (which is consistent with Figure 2).

Figure 4 shows the measured $\beta_{\lessgtr 0}$ as functions of the inner location $y_i$ for two outer locations ($y_o^+ = 215$ and 400). Again, the large scales at the inner location are modeled using $\alpha u'_o$, with no sign-dependent conditioning for superposition. We make a few observations. The observed difference between $R_{\lessgtr 0}$ in Figure 2 (d) is found as well in $\beta_{\lessgtr 0}$, confirming that $R_{\lessgtr 0} \sim \beta_{\lessgtr 0}$. $\beta_{\lessgtr 0}$ are more accurately predicted than $\beta$ (Figure 1). Equation (3.4), however, is still successful only within the viscous sublayer.

The usefulness of Eq. (1.3) depends on whether the large scale can be commensurate with the resolved flow field. As such, sensitivities in the implications of this analysis to $l$ should be minimal. Therefore, we, have repeated the above analysis for a different filtering length scale, $l^+ = 7000$. Figure 5 shows the measured response function as functions of $u'_L$. Similar results are obtained; the qualitative trends of the response function do not seem to be strongly dependent on $l$. This result is consistent with the findings for $\beta$ for temporal amplitude modulation (Mathis *et al.* 2011).

In this subsection, we have directly measured the response function $f$ as functions of the wall-normal distance and the large-scale fluctuation $u'_L$. We have shown that the response function can be approximated by the piece-wise linear function of Eq. (3.1). Furthermore, the response function collapses for all $Re_\tau$ considered (2000—13000). Coupling the equilibrium assumption with the HRAP, the PIO model is now fully predictive ($\alpha$ and $\beta$ are known). Statistical details of $G$ (or $u_i^*$) other than $\mu$ and $\sigma^2$, however, still require further investigation. In particular, $\langle G^3 \rangle \neq 0$ and must be modeled. The refined PIO model, which accounts for the asymmetry of $\beta$, should be used to correctly resolve the spatial amplitude modulation in the prediction of $u'$.

### 3.2. *Positive and negative amplitude modulation*

The small scales in the near-wall region are subject to changes in the local Reynolds number, which are dominated by large-scale fluctuation. Equations (2.8) and (3.4) model amplitude modulation due to this effect. According to the HRAP, a large-scale eddy affects the entire region beneath it (see e.g. Yang *et al.* 2016*c*; Yang & Lozano-Durán 2017; Yang *et al.* 2017). Therefore, it is unlikely that the amplitude modulation due to changes

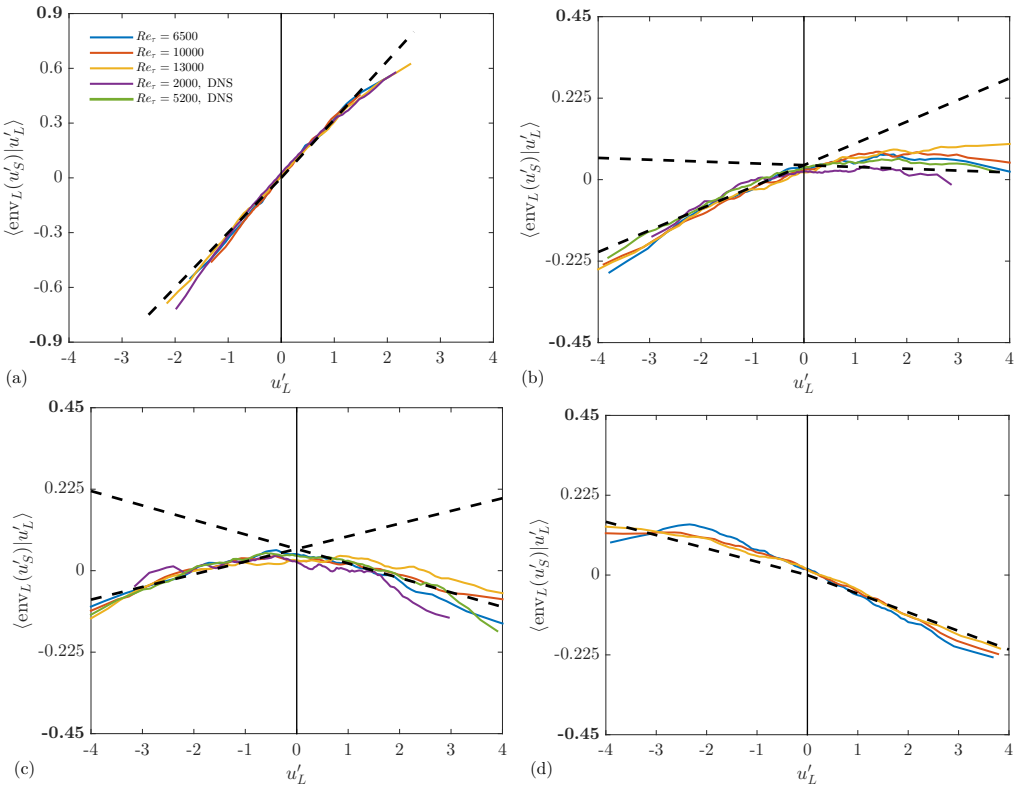


FIGURE 5. (a-c) Same as in Figure 2 except with $l^+ = 7000$. (d) Same as in (a-c) except with $y/\delta = 0.2$. The linear fits are the same as in Figure 2.

in the local Reynolds number would be a function of the wall-normal distance. This expectation is expressed explicitly in both Eq. (2.8) and Eq. (3.4), where the predicted response function is not a function of $y_i$. The measured response function $f(u'_L)$ (Figures 2, 3, and 5), however, is an integrated parameterization of the small-scale responses to the large-scale fluctuation. As such, the response function accounts for the amplitude modulation due to changes in the local Reynolds numbers as well as other physical mechanisms that seemingly lead to negative amplitude modulation. This apparent negative modulation increases as a function of $y^+$.

The physical mechanisms behind the negative amplitude modulation were discussed by Agostini & Leschziner (2014) and Baars *et al.* (2017). We argue that such mechanisms compete with the positive amplitude modulation and lead to the overall behavior of the response function that is observed in Figures 2-5. While in the viscous region, such mechanisms are not of great importance, they become stronger away from the wall, resulting in a decrease in the amplitude modulation strength for both $u'_L < 0$ and $u'_L > 0$ (i.e., a decrease in $\beta_{\lessgtr 0}$). Moreover, because a fluid in the bulk regions generally flows at high speeds, intrusions of such fluid into the near-wall region lead to positive large-scale velocity fluctuation. As a result, $\beta_{>0}$ decreases more rapidly than $\beta_{<0}$ as a function of the wall-normal distance. At the top of the log layer and in the bulk region, the effect of the positive amplitude modulation driven by the local $Re_\tau$ is no longer present.

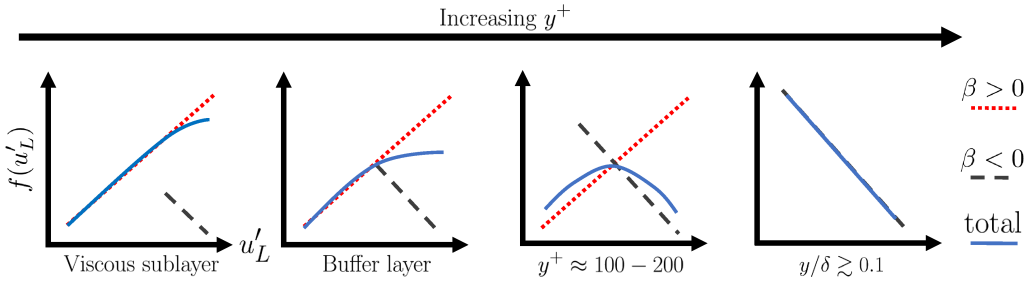


FIGURE 6. The qualitative shape of the conditional average profiles can be seen as a superposition of the positive amplitude modulation (dotted) which is predicted by the hierarchical random additive process (HRAP) and the negative amplitude modulation (dashed). The negative amplitude modulation is likely the role of sweeps and ejections. These effects combine to create the profile shape seen in Figures 2-5 (solid). The influence of ejections becomes more significant away from the wall, where the effect of the one-sided flow constriction is relaxed. As a result, the HRAP's prediction of amplitude modulation will become less accurate as a function of $y^+$.

Additionally, the negative amplitude modulation is likely less significant for $u'_L < 0$ due to the confinement of the wall from below. Due to the presence of the wall, the role of ejections on the small-scale energetics will be less significant than the role of sweeps in the near-wall region. This competition between the two mechanisms at the various boundary-layer locations is sketched in Figure 6.

## 4. Conclusions

In this report, we have investigated inter-scale interaction in turbulent flows. We directly measured the response function of small-scale velocity fluctuation in Eq. (1.2) in wall-bounded flows as functions of the wall-normal distance and the large-scale velocity fluctuation. Although a linear response function as suggested by Marusic *et al.* (2010) is not valid outside of the viscous sublayer, a piecewise linear function Eq. (3.1) is a good approximation of the response function in wall turbulence. Furthermore, positive amplitude modulation is shown to be invariant of the wall-normal height of the inner location and to the Reynolds number. We have carefully assessed usefulness of Eq. (1.3) in the context of WMLES. We argue that it is possible to correspond the large and small scales to the resolved and unresolved turbulence in the near-wall region for a typical WMLES. Therefore, the model of Eq. (1.3) can be useful to LES wall modeling if the modeling parameters can be specified in a non-empirical manner using Eq. (2.8). One specification is ventured in Section 2, and the prediction agrees reasonably well with the measurements in the viscosity-dominated region (which is the region of interest if the wall-shear stress is the quantity to be modeled). We observed that inter-scale interaction is an integrated effect of positive amplitude modulation and negative amplitude modulation. Although we have limited our discussion to the streamwise velocity fluctuation, this discussion is likely to be relevant to wall-shear stress and spanwise and vertical velocity components as well (Talluru *et al.* 2014).

**Acknowledgements**

This work is funded by AFOSR, Grant #1194592-1-TAAHO. The first author is also supported by a National Science Foundation Graduate Research Fellowship under Grant #DGE-1656518 and a Stanford Graduate Fellowship.

REFERENCES

Agostini, L., Leschziner, M. & Gaitonde, D. 2016 Skewness-induced asymmetric modulation of small-scale turbulence by large-scale structures. *Phys. Fluids* **28**, 015110.

Agostini, L. & Leschziner, M. A. 2014 On the influence of outer large-scale structures on near-wall turbulence in channel flow. *Phys. Fluids* **26**, 075107.

Baars, W. J., Hutchins, N. & Marusic, I. 2017 Reynolds number trend of hierarchies and scale interactions in turbulent boundary layers. *Phil. Trans. R. Soc. A* **375**, 1-18.

Baars, W. J., Talluru, K. M., Hutchins, N. & Marusic, I. 2015 Wavelet analysis of wall turbulence to study large-scale modulation of small scales. *Exp. Fluids* **56**, 188–203.

Bandyopadhyay, P. R. & Hussain, A. 1984 The coupling between scales in shear flows. *Phys. Fluids* **27**, 2221–2228.

Berkooz, G., Holmes, P. & Lumley, J. L. 1993 The proper orthogonal decomposition in the analysis of turbulent flows. *Annu. Rev. Fluid Mech.* **25**, 539–575.

Bose, S. T. & Park, G. I. 2017 Wall-modeled les for complex turbulent flows. *Annu. Rev. Fluid Mech.* **50**.

Brown, G. L. & Thomas, A. S. W. 1977 Large structure in a turbulent boundary layer. *Phys. Fluids* **20**, 243–252.

Chernyshenko, S. I., Marusic, I. & Mathis, R. 2012 Quasi-steady description of modulation effects in wall turbulence. In arXiv preprint, arXiv:1203.3714.

Fiscaletti, D., Ganapathisubramani, B. & Elsinga, G. E. 2015 Amplitude and frequency modulation of the small scales in a jet. *J. Fluid Mech.* **772**, 756–783.

Ganapathisubramani, B., Hutchins, N., Monty, J. P., Chung, D. & Marusic, I. 2012 Amplitude and frequency modulation in wall turbulence. *J. Fluid Mech.* **712**, 61–91.

Hoyas, S. & Jiménez, J. 2006 Scaling of the velocity fluctuations in turbulent channels up to $\mathrm{Re}_\tau = 2003$. *Phys. Fluids* **18**, 011702.

Hutchins, N., Chauhan, K., Marusic, I., Monty, J. & Klewicki, J. 2012 Towards reconciling the large-scale structure of turbulent boundary layers in the atmosphere and laboratory. *Boundary-Layer Meteorol.* **145**, 273–306.

Hutchins, N. & Marusic, I. 2007 Large-scale influences in near-wall turbulence. *Phil. Trans. R. Soc. A* **365**, 647–664.

Hutchins, N., Monty, J. P., Ganapathisubramani, B., Ng, H. C. H. & Marusic, I. 2011 Three-dimensional conditional structure of a high-Reynolds-number turbulent boundary layer. *J. Fluid Mech.* **673**, 255–285.

Hutchins, N., Nickels, T. B., Marusic, I. & Chong, M. 2009 Hot-wire spatial resolution issues in wall-bounded turbulence. *J. Fluid Mech.* **635**, 103–136.

Inoue, M., Mathis, R., Marusic, I. & Pullin, D. I. 2012 Inner-layer intensities for the flat-plate turbulent boundary layer combining a predictive wall-model with large-eddy simulations. *Phys. Fluids* **24**, 075102.

Jiménez, J. & Pinelli, A. 1999 The autonomous cycle of near-wall turbulence. *J. Fluid Mech.* **389**, 335–359.

Johnson, P. L. & Meneveau, C. 2017 Turbulence intermittency in a multiple-time-scale Navier-Stokes-based reduced model. *Phys. Rev. Fluids* **2**, 072601.

Lee, M. & Moser, R. D. 2015 Direct numerical simulation of turbulent channel flow up to $\mathrm{Re}_\tau \approx 5200$. *J. Fluid Mech.* **774**, 395–415.

Li, Y., Perlman, E., Wan, M., Yang, Y., Meneveau, C., Burns, R., Chen, S., Szalay, A. & Eyink, G. 2008 A public turbulence database cluster and applications to study lagrangian evolution of velocity increments in turbulence. *J. Turbul* **9**, N31, 1–29.

Marusic, I. & Heuer, W. D. 2007 Reynolds number invariance of the structure inclination angle in wall turbulence. *Phys. Rev. Lett.* **99**, 114504, 1-4.

Marusic, I., Mathis, R. & Hutchins, N. 2010 Predictive model for wall-bounded turbulent flow. *Science* **329**, 193–196.

Mathis, R., Hutchins, N. & Marusic, I. 2009*a* Large-scale amplitude modulation of the small-scale structures in turbulent boundary layers. *J. Fluid Mech.* **628**, 311–337.

Mathis, R., Hutchins, N. & Marusic, I. 2011 A predictive inner-outer model for streamwise turbulence statistics in wall-bounded flows. *J. Fluid Mech.* **681**, 537–566.

Mathis, R., Marusic, I., Chernyshenko, S. I. & Hutchins, N. 2013 Estimating wall-shear-stress fluctuations given an outer region input. *J. Fluid Mech.* **715**, 163-180.

Mathis, R., Monty, J. P., Hutchins, N. & Marusic, I. 2009*b* Comparison of large-scale amplitude modulation in turbulent boundary layers, pipes, and channel flows. *Phys. Fluids* **21**, 111703.

McKeon, B. 2017 The engine behind (wall) turbulence: perspectives on scale interactions. *J. Fluid Mech.* **817**, 1-86.

Meneveau, C. & Katz, J. 2000 Scale-invariance and turbulence models for large-eddy simulation. *Annu. Rev. Fluid Mech.* **32**, 1–32.

Moin, P., Squires, K., Cabot, W. & Lee, S. 1991 A dynamic subgrid-scale model for compressible turbulence and scalar transport. *Phys. Fluids* **3**, 2746–2757.

Perry, A. E., Henbest, S. & Chong, M. 1986 A theoretical and experimental study of wall turbulence. *J. Fluid Mech.* **165**, 163–199.

Perry, A. E. & Marusic, I. 1995 A wall-wake model for the turbulence structure of boundary layers. Part 1. extension of the attached eddy hypothesis. *J. Fluid Mech.* **298**, 361–388.

Piomelli, U. & Balaras, E. 2002 Wall-layer models for large-eddy simulations. *Annu. Rev. Fluid Mech.* **34**, 349–374.

Rao, K. N., Narasimha, R. & Narayanan, M. A. B. 1971 The "bursting" phenomenon in a turbulent boundary layer. *J. Fluid Mech.* **48**, 339–352.

Schmid, P. J. 2010 Dynamic mode decomposition of numerical and experimental data. *J. Fluid Mech.* **656**, 5–28.

Sharma, A. & McKeon, B. 2013 On coherent structure in wall turbulence. *J. Fluid Mech.* **728**, 196–238.

Sidebottom, W., Cabrit, O., Marusic, I., Meneveau, C., Ooi, A. & Jones, D. 2014 Modelling of wall shear-stress fluctuations for large-eddy simulation. In *Proc. 19th Australasian Fluid Mechanics Conference*.

Silvis, M. H., Remmerswaal, R. A. & Verstappen, R. 2017 Physical consistency

of subgrid-scale models for large-eddy simulation of incompressible turbulent flows. *Phys. Fluids* **29**, 015105.

Smits, A. J., McKeon, B. J. & Marusic, I. 2011 High–reynolds number wall turbulence. *Annu. Rev. Fluid Mech.* **43**, 353–375.

Talluru, K. M., Baidya, R., Hutchins, N. & Marusic, I. 2014 Amplitude modulation of all three velocity components in turbulent boundary layers. *J. Fluid Mech.* **746**, R1.

Towne, A., Schmidt, O. T. & Colonius, T. 2017 Spectral proper orthogonal decomposition and its relationship to dynamic mode decomposition and resolvent analysis. *J. Fluid Mech.* **825**, 1113–1152.

Townsend, A. A. 1976 *The Structure of Turbulent Shear Flow*. Cambridge University Press.

Yang, X. I. A., Baidya, R., Johnson, P., Marusic, I. & Meneveau, C. 2017 Structure function tensor scaling in the logarithmic region derived from the attached eddy model of wall-bounded turbulent flows. *Phys. Rev. Fluids* **2**, 064602.

Yang, X. I. A. & Howland, M. F. 2018 Implication of Taylor's hypothesis on measuring flow modulation. *J. Fluid Mech.* **836**, 222-237.

Yang, X. I. A. & Lozano-Durán, A. 2017 A multifractal model for the momentum transfer process in wall-bounded flows. *J. Fluid Mech.* **824**, R2.

Yang, X. I. A., Marusic, I. & Meneveau, C. 2016*a* Hierarchical random additive process and logarithmic scaling of generalized high order, two-point correlations in turbulent boundary layer flow. *Phys. Rev. Fluids* **1**, 024402.

Yang, X. I. A., Marusic, I. & Meneveau, C. 2016*b* Moment generating functions and scaling laws in the inertial layer of turbulent wall-bounded flows. *J. Fluid Mech.* **791**, R2.

Yang, X. I. A., Meneveau, C., Marusic, I. & Biferale, L. 2016*c* Extended self-similarity in moment-generating-functions in wall-bounded turbulence at high Reynolds number. *Phys. Rev. Fluids* **1**, 044405.

Zhang, C. & Chernyshenko, S. I. 2016 Quasisteady quasihomogeneous description of the scale interactions in near-wall turbulence. *Phys. Rev. Fluids* **1**, 014401.